Special Issue
Frontier in Characterization of Materials and Processes for Steel Manufacturing

ISIJ International, Vol. 62 (2022), No. 5, pp. 977–983
https://doi.org/10.2355/isijinternational.ISIJINT-2021-409

Local Structure Investigation of Cu Precipitates in Modified 18CrNiMo7-6 Steels by Synchrotron X-ray Absorption Spectroscopy

Piyada SUWANPINIJ,[1)]* Margarita BAMBACH,[2)] Atipong BOOTCHANONT[3,5)] and Wutthigrai SAILUAM[4)]

1) The Sirindhorn International Thai-German Graduate School of Engineering (TGGS), King Mongkut's University of Technology North Bangkok (KMUTNB). Now at Working Group Metallurgy and Metal Forming, Leibniz-Institut für Werkstofforientierte Technologien (IWT), Badgasteiner Straße 3, Bremen, 28359 Germany.
2) Gesellschaft für Metallurgische Technologie- und Softwareentwicklung mbH (GMT), Börnicker Chaussee 1–2, Bernau, 16321 Germany.
3) Smart Materials Research Unit, Division of Physics, Faculty of Science and Technology, Rajamangala University of Technology Thanyaburi, Pathumthani, 12110 Thailand.
4) Rajamangala University of Technology ISAN (Khon Kaen Campus), 150 Srichan Road Muang, KhonKaen, 40000 Thailand.
5) Division of Physics, Faculty of Science and Technology, Rajamangala University of Technology Thanyaburi, Pathumthani, 12110 Thailand.

(*Received on September 8, 2021; accepted on December 8, 2021*)

This paper studied the copper precipitation in an 18CrNiMo7-6 martensitic steel (0.19 mass% C) with copper addition and its resulting improved mechanical behavior. The development of nano-precipitates in two modified alloys with 1.0 and 1.5 mass% copper addition was investigated by means of synchrotron X-ray absorption spectroscopy. The first-principles calculation has enabled the modeling of the unavailable copper standards: solid solution, B2, BCC, 2H, 9R and 3R, for calculating the XAS spectra and successfully identified the unknown phases after aging for the first time in this steel group. The samples alloyed with 1.5 mass% copper yielded the semi-coherent 9R structure when aged at 500°C between 166 to 360 minutes. The ones containing 1 mass% copper formed the B2 ordered structure after aging at 480°C for 50 minutes and revealed the co-existence of the 9R after 240 minutes. The analysis reveals the precipitation kinetics of copper in low carbon martensitic steel and helps determine the optimum tempering parameters to adjust peak strength.

KEY WORDS: X-ray absorption spectroscopy; copper precipitation; 18CrNiMo7-6 steel; B2 ordered structure; semi-coherent 9R structure; first-principles calculation.

1. Introduction

The copper precipitation mainly in Fe–Cu based systems and very low carbon ferritic steels has been studied extensively in the literature[1–11)] whereas there is very little information about copper-alloyed low carbon steels. Improved strengths, high strain hardening rates during static and cyclic loading as well as extended elongation under tension have been reported for a copper-alloyed 18CrNiMo7-6 steel for gearbox applications due to the nano-precipitates of copper after aging.[12)] Some improved tensile properties from the former works[12,13)] will be recalled here for discussion. The conventional Transmission Electron Microscopy (TEM) could not prove their presence so far whereas the advanced method such as Small Angle Neutron Scattering (SANS) was able to prove the average size of the precipitates in the investigated compositions.[12,13)] The SANS, nevertheless, cannot yield any information on the crystal structure of the precipitates or their orientation relationship with the matrix. The latter is important to better understand the strain hardening behavior during monotonic and cyclic loading of the steels and to tailor their properties so that the service life of components can be extended.

It is well-known that the low solubility of copper in ferrite allows the precipitation of copper in iron alloys at nominal copper content higher than 0.7 mass% after aging at 400–650°C.[1,14)] **Figure 1** represents the different possible forms of copper precipitates in iron alloys. Before the onset of precipitation, copper atoms substitute the iron atoms randomly within the solid solution. At the infant stage of precipitation, the copper atoms start losing the randomness in the solid solution by substituting one iron atom in the

* Corresponding author: E-mail: suwanpinij@iwt-bremen.de

middle of each unit cell. This stage is called B2 ordered structure or cluster as reported recently[15–17] with the average radius of 2 nm.[17] The BCC copper phase, whose maximum radius lies between 2 to 4 nm,[4] forms when copper substitutes all iron atoms in the unit cell. The precipitates lose their coherency partially when growing and transforming into the twinned monoclinic martensitic 9R phase, with a radius size of 3.5–7.5 nm.[6] Wang *et al.* reported the co-existence of a twinned hexagonal close-packed 2H variant with much smaller unit cell in the same precipitate, besides the 9R structure.[18] The 9R structure turns into semi-coherent ellipsoidal Cu-rich precipitates or the so-called 3R structure with orthorhombic unit cell[19] at a range of radius between 9 to 15 nm.[9,20] Finally, the stable, fully incoherent, ε-FCC copper precipitates are formed at the radius larger than 20 nm.[10] Rassoul[21] as well as Jung *et al.*[22] reported the decelerated copper precipitation transformation kinetics due to increased carbon content. The carbon content in the investigated 18CrNiMo7-6 is 0.19 mass%, significantly higher than almost all other systems studied in the literature. X-ray Absorption Near Edge Spectroscopy (XANES) and Extended X-Ray Absorption Fine Structure (EXAFS) spectra has become the key for phase identification and has successfully solved the complexity in this paper. Several papers[23–25] employed the X-ray absorption spectroscopy (XAS) technique in identifying the evolution of cubic copper phases, but either the investigated systems were very low carbon steels or binary Fe–Cu. The phase identification of the copper precipitates in the 18CrNiMo7-6 steel has not been performed by XAS coupled with the first-principles calculation before, up to the knowledge of the authors.

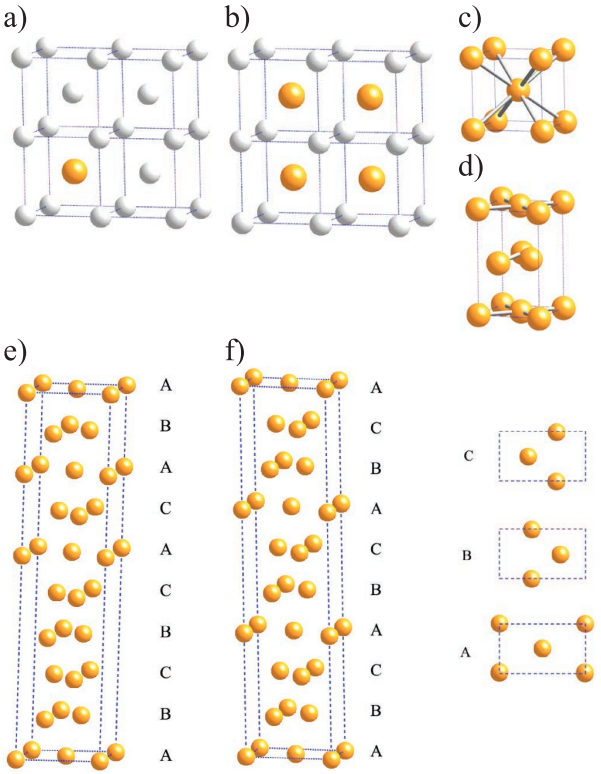

Fig. 1. The sequence of the evolution of the copper precipitates in iron alloys; a) solid solution and b) B2 ordered structure in 4 unit cells; c) BCC; d) 2H; e) 9R; f) 3R. The gray spheres represent Fe atoms, and larger orange spheres represent Cu atoms. (Online version in color.)

2. Experimental Details

2.1. Materials and Heat Treatments

The standard 18CrNiMo7-6 steel was modified by adding 1.5 and 1.0 mass% copper and named as 18CrNiCuMo7-6-15 and 18CrNiCuMo7-6-10, respectively. More information regarding the metallurgical processing of the steel and the following pre-forming is available elsewhere.[12,13] The nominal chemical compositions of the studied steels determined by Optical Emission Spark Spectroscopy (OES) are given in **Table 1**. The aluminum content was measured by wet chemical analysis whereas the amounts of nitrogen and oxygen were determined by the carrier gas method.

The thermal cycle started with 2-step solution annealing at 940°C (60 and 30 minutes) followed by 850°C for 10 minutes before quenching in oil for 15 minutes to stimulate the case hardening process. The subsequent aging at 500 and 480°C in this work, for the 18CrNiCuMo7-6-15 and 18CrNiCuMo7-6-10 alloys, respectively, simulated high temperature tempering in martensitic steel and will be under the focus of research. The aging durations were varied from aging, in order to obtain a peak cyclic strain hardening coefficient in each composition, to overaging (see **Table 2**) as were determined in previous analysis.[12]

2.2. The XAS Measurement

The XAS measurements were carried out at beamline BL8 of the Siam Photon Laboratory (SPL) at Synchrotron Light Research Institute (SLRI), Nakhon Rachasima, Thailand, similar to a previous work.[26] The SPL ring operates with an electron energy of 1.2 GeV with a beam current of 150–80 mA. All the mirror-polished samples were scanned for Cu *K*-edge absorption spectra in fluorescent mode, making an angle between to the sample surface and to the detector at 45°. The incoming beam with a cross

Table 2. The aging treatment of the studied samples.

Samples	Alloy Name	Aging Parameters
1.5/O	18CrNiCuMo7-6-15	Overaged at 500°C for 360 min
1.5/A		Aged at 500°C for 166 min
1.0/O	18CrNiCuMo7-6-10	Overaged at 480°C for 240 min
1.0/A		Aged at 480°C for 50 min

Table 1. The nominal compositions in mass% of the copper-added 18CrNiCuMo7-6-15 and 18CrNiCuMo7-6-10 alloys.

Name	C	Si	Mn	P	S	Cr	Mo	Ni	Al	Cu	N	O
18CrNiCuMo7-6-15	0.185	0.34	0.59	0.004	0.021	1.53	0.270	1.73	0.045	1.45	0.014	0.0008
18CrNiCuMo7-6-10	0.195	0.31	0.57	0.003	0.026	1.50	0.265	1.52	0.043	0.97	0.012	0.0010

section of 1 × 16 mm penetrating down to 100 μm results in an illuminated volume of 1.6 mm^3.[26] The detector used in the fluorescent mode is made of highly sensitive 13 germanium elements.

A thin copper foil was scanned in the transmission mode to provide a standard spectrum of the ε-FCC phase using a 40-cm long chamber containing a gas mixture of argon and helium with a pressure of 1 MPa. In addition, XANES/EXAFS spectra of the other copper forms were calculated by the first-principles calculation as will be described in the following section.

3. The First-principles and XAS Calculation

All structural models are constructed from the Density Functional Theory (DFT) by using projector augmented wave (PAW) method.[27] The generalized gradient approximations (GGA)[28] from is used to describe exchange correlation, as implement in the Vienna Ab initio Simulation Package (VASP).[29] The plane wave cutoff was set at 520 eV. Special sampling points in the Brillouin zone were generated by the Monkhorst-Pack scheme,[30] and a k-point mesh of 9 × 9 × 3 was used for BCC, 9R and 3R structures, whereas that of 5 × 5 × 5 was set for the 2H. The structural models of B2 (Cu 27 atoms and Fe 27 atoms) and solid solution (Cu 1 atom and Fe 53 atoms) structures were performed by using a 3 × 3 × 3 supercell with 54 atoms of Fe unit cell (BCC; space group $Im\bar{3}m$) and 2 × 2 × 2 k-points grid meshes for Brillouin zone integrations. The tolerances for all geometry optimization are set as the difference between cycles in total energy and force being 0.1 meV/nm and 0.1 meV, respectively. All crystal structures are shown in Fig. 1.

The obtained structures from DFT were used to simulate XANES/EXAFS spectra by using the FEFF code utilizing a full multiple scattering approach based on ab initio overlapping muffin–tin potentials.[31] The muffin–tin potentials used in the FEFF code are self-consistent calculations with the Hedin–Lundqvist exchange-correlation function.[32] The XANES/EXAFS spectra of copper were calculated in a spherical radius of 0.5 nm and the full multiple scattering calculations include all possible paths within a larger cluster radius of for all models. The Cu K-edge XANES/EXAFS simulated spectra were then obtained using the FEFF9 code for all structures.

4. Results

The normalized EXAFS spectra in E and k-spaces of all four samples are depicted in **Fig. 2**. To process and enhance the EXAFS signal in the high k-region, they are plotted with $k^2\chi(k)$. Larger differences between the samples can be seen in the XANES region despite the high similarity in samples 1.5/A and 1.5/O. The self-absorption correction in Athena yields identical spectra due to the very low concentration of copper in the samples. In **Fig. 3**, all the simulated EXAFS spectra in E and k-spaces of the 3R, 9R, 2H, BCC, B2 and solid solution are plotted together with the ε-FCC from copper foil.

To help identify the phase in each sample, the XANES spectra are plotted in E-space until 9 050 eV and compare the possible structures as displayed in **Figs. 4** and **5**. It is rather clear that both the 1.5/A and 1.5/O contain the same structure, 9R, resembling the characteristic hump at short before 9 000 eV. The sample 1.0/A, after the optimum aging, matches well with the XANES spectrum from the B2 ordered structure and infers containing purely this structure. The 1.0/O exhibits the flattening in the oscillation at 8 990 and behind 9 010 eV and implies the possibility of co-existence of other phases after the overaging.

Possible conclusions are that, (i) the 1.0/A tends to form only the B2 ordered structure while (ii) the sample 1.5/O contains only the 9R structure. To prove if the 1.0/O con-

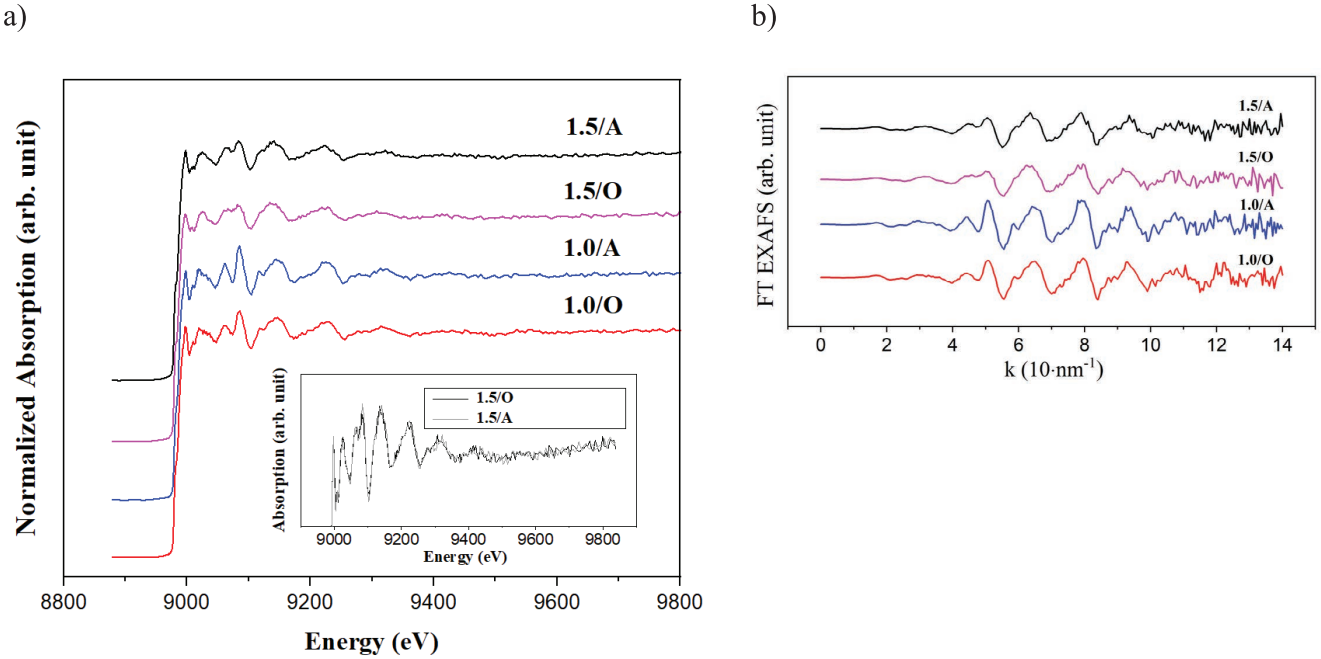

Fig. 2. The EXAFS spectra of all investigated sample in a) E and b) k-spaces. The samples 1.5/A and 1.5/O are compared in the small window showing the very high similarity. (Online version in color.)

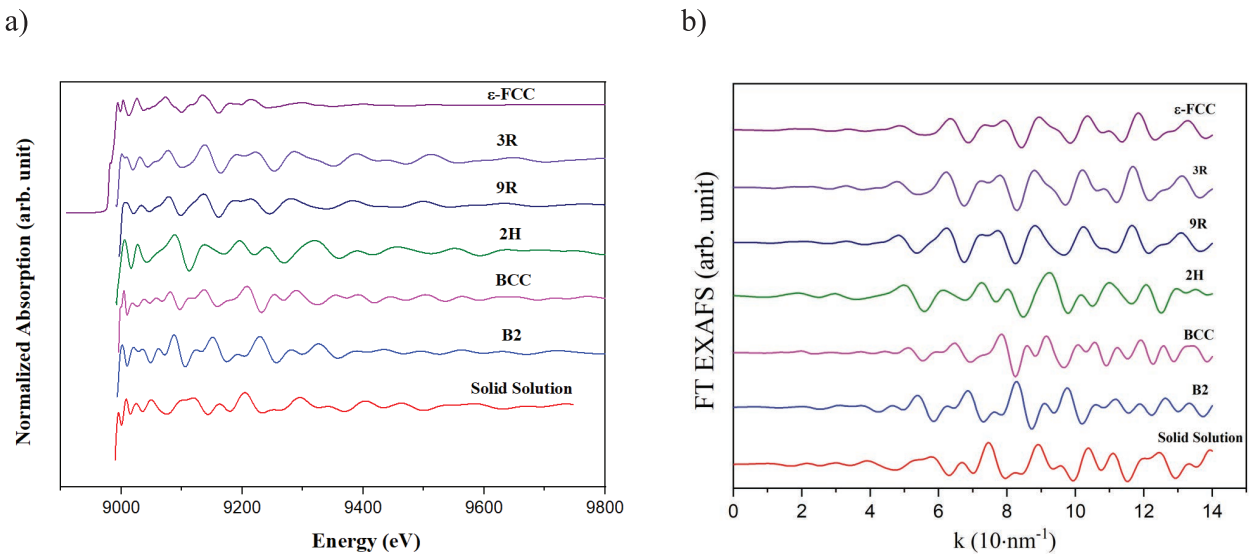

Fig. 3. The EXAFS spectra of all modeled structures in a) *E* and b) *k*-spaces, compared with the *ε*-FCC from copper foil. (Online version in color.)

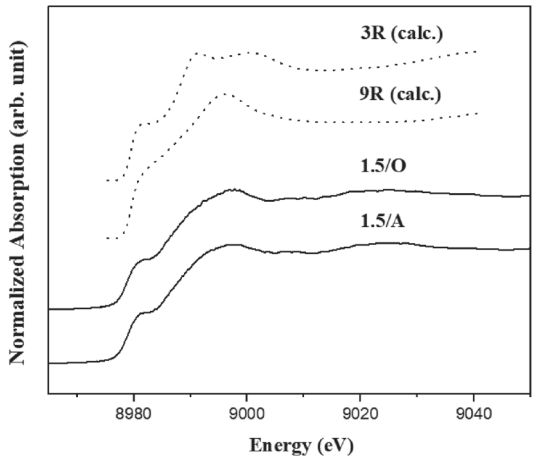

Fig. 4. The XANES spectra of the 1.5/O and 1.5/A, compared with the modeled 9R and 3R structure in dash lines.

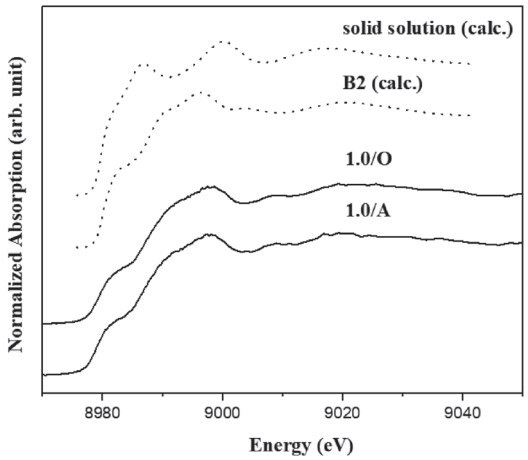

Fig. 5. The XANES spectra of the 1.0/A and 1.0/O compared with the modeled B2 and solid solution structure in dash lines.

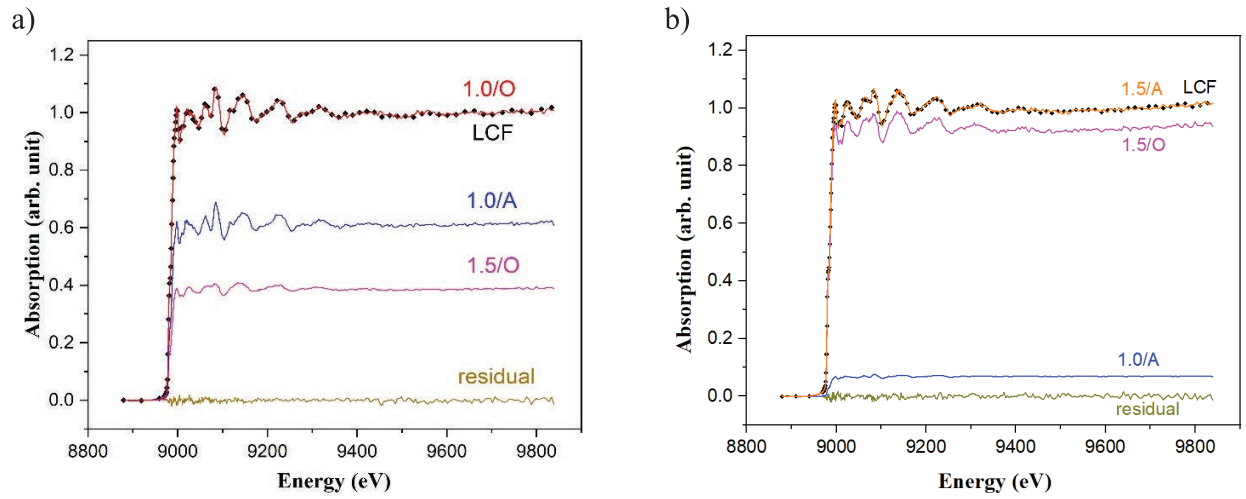

Fig. 6. The LCF result of the a) 1.0/O and b) 1.5/A samples, with the weighted fractions of the 1.0/A and 1.5/O fitting standards (as B2 and 9R structures), and the residual. (Online version in color.)

tains the co-existence of 9R structure, the Linear Combination Fit (LCF) method was employed to resolve its possible fraction the 1.0/A and 1.5/O as standards for the B2 and 9R structures, respectively. Please note that the modeled spectra are not valid as fitting standards for LCF. **Figure 6**(a) reveals the LCF results, yielding 61.3% of the 1.0/A

and 38.7% of 1.5/O sample with very small fractional misfit $\left(\mathrm{R}, \frac{\sum((data-fit)^2)}{\sum(data^2)}\right)$ of 0.0003078. This means that the overaged sample of 1.0/O forms a mixture of the B2 ordered structure and 9R twinned martensitic copper phase with the atomic ratio of 61.3 to 38.7. The LCF of the 1.5/A sample, in contrast, confirms a very low amount of 6.9 atomic% of the B2 structure in the 1.5/A sample, as plotted in Fig. 6(b), with a very low R value of 0.0004567.

5. Discussion

In order to gain more insight in the phase shift in all samples, the EXAFS spectra should be also analyzed in *R*-space. **Figure 7** plots the EXAFS spectra of the samples, compared with the calculated B2 and 9R structures, taken the *k*-range of 0.3–1.0 nm. The experimental FT-XAFS feature of the 1.0/A sample is similar to the calculated spectrum for the copper atom in the B2 structure obtained using the FEFF code. This result implies that the peak around 0.1–0.3 nm in 1.0/A sample is considered as a Cu–Fe bonding, which will decrease while the bonding transforms to Cu-Cu in the 9R structure. Likewise, with increasing the copper contents, the feature of FT-XAFS spectra around 0.3–0.5 nm in the 1.5/O sample decreases and becomes similar to the 9R structure. However, the 1.0/O and 1.5/A samples still exhibit the features of B2 cluster, which corresponds to the LCF in Fig. 6.

We can now summarize the XAS results and compare with our previously published results from SANS as tabulated in **Table 3**. The XANES/EXAFS identified the copper structures as the ordered B2 and martensitic 9R. After the extra long overaging period of 6 hours at 500°C in the 18CrNiCuMo7-6-15 grade (1.5/O), the small fraction of the B2 structure transforms completely into the semi-incoherent twinned 9R structure and only the 9R phase remains. Somewhat higher noise in the 1.5/A sample could arise from the decreasing X-ray flux along the beamtime as this sample was scanned after the 1.5/O. The SANS technique detected the precipitates of copper in the 1.5/A sample with an average radius of 3.159 nm.[13] This is in fair agreement with the literature stating that the 9R structure starts from a radius of 3.5 nm.[6] The 1.5/O sample possibly contains larger size of the 9R precipitates due to the overaging treatment. However, such difference in size cannot be detected by XAS because the scattered X-ray from the neighboring atoms only within 0.8 nm, *i.e.*, three unit cells of BCC iron, can contribute to the EXAFS spectra. In the 18CrNiCuMo7-6-10 grade, the SANS also detected a smaller precipitate radius of 1.650 nm in the aged sample (1.0/A).[12,13] This radius size corresponds to the coherent BCC structure in the literature before the B2 structure has been investigated intensively. After the long overaging time of 240 minutes, some B2 cluster becomes 9R martensite.

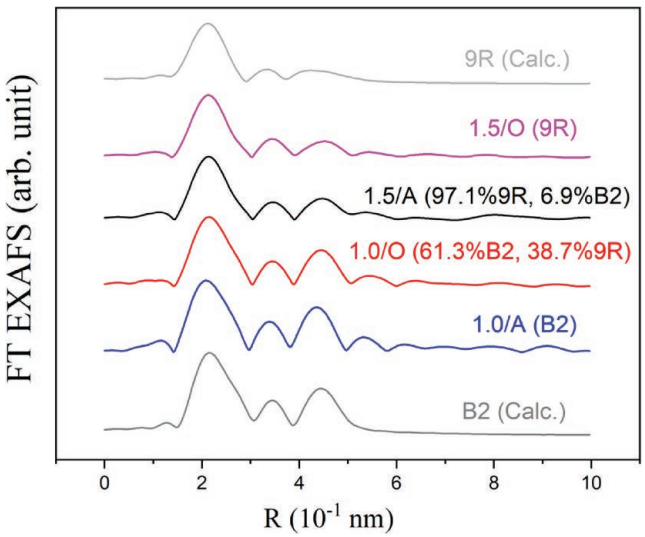

Fig. 7. FT-XAFS spectra, plotted to compare with the simulated B2 and 9R structures. (Online version in color.)

The stress-strain curves reported in our previous publications[12,13] are replotted in **Fig. 8**(a) for further discussion. The benchmark material is the standard 18CrNoMi7-6 steel without copper addition under the same aging parameters for comparison. It is designated with temperature/time. Here, the aging acts as a high temperature tempering that recovers the ductility and toughness for the martensitic matrix at the expense of significant drop in the yield (YS) and tensile strengths (UTS) while forming copper precipitates. This point is the fact that the peak strength cannot be indicated easily by tempering curves. The increase in YS by 1.0 mass% copper addition after aging at 480°C for 50 minutes (1.0/A) is as high as 124 MPa, accounted for 11.6% increase from the benchmark. On the other hand, its UTS is improved in a lesser degree, *i.e.*, 72 MPa. A similar trend is seen in the 1.5/A sample, aged at a higher temperature of 500°C for 166 minutes, with a significantly lower improvement in both YS and UTS according to the longer tempering period but with superior ductility.

The material behavior under cyclic loading is not only influenced by its static strength but also by the strain hardening potential. The latter becomes relevant when local plastic flow (microyielding) occurs due to the different deformation

Table 3. Summary of the XAS results and additional information from SANS.

Sample	Copper content [mass%]	Thermal history	XAS results	SANS results
1.5/O	18CrNiCuMo7-6-15	Overaged at 500°C for 360 min	9R	N/A
1.5/A		Aged at 500°C for 166 min	93.1% of 9R, 6.9% of B2	Radius of 3.159 nm with a volume of 1.16% by SANS[13]
1.0/O	18CrNiCuMo7-6-10	Overaged at 480°C for 240 min	61.3% of B2, 38.7% of 9R	N/A
1.0/A		Aged at 480°C for 50 min	B2	Radius of 1.650 nm by SANS[12]

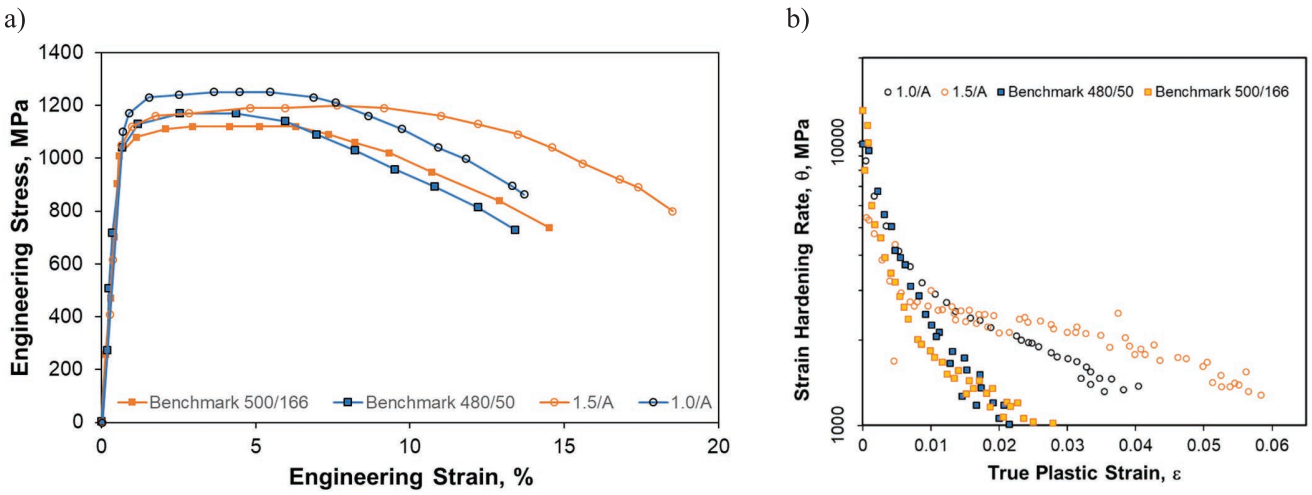

Fig. 8. a) The engineering stress-strain curves and b) the strain hardening rate, $\left(\frac{d\sigma}{d\varepsilon}\right)$,[13] of the benchmark 18CrNiMo7-6 alloy compared with its copper-added variations with the same aging parameters. (Online version in color.)

behavior of *e.g.* non-metallic inclusions versus the matrix. It needs to be assessed together with its strength in order to predict its resistance to fatigue. Figure 8(b) replots the strain hardening rate, $\left(\frac{d\sigma}{d\varepsilon}\right)$, of the same samples as a function of the true plastic strain. It is clear that the copper precipitates assist the strain hardening from the strain of 0.01. The lower strength 1.5/A sample exhibits superior strain hardening rate to the 1.0/A sample. Both copper-added alloys reveal larger ductility, which is most pronounced in the 1.5/A sample. This is preferable for damage tolerant design in components withstanding a large number of cyclic loads, such as gearboxes. In contrast, the condition 1.0/A with an increase in the yield strength is rather suitable for safe life design.

The observed mechanical properties reflect the different strengthening mechanisms from B2 and 9R phases. The former produces the so-called ordered domain strengthening by generating anti-phase boundaries as reported by Han *et al.*[17] The lower yield strength improvement here (*ca.* 120 MPa in the 1.0/A sample compared with *ca.* 220 MPa in Han *et al.*[17] can be explained by the lower copper content (1.0 mass% compared with 2.1 mass% by Han *et al.*[17]). Moreover, in our case, only little improved work hardening arises as the dislocations already cut through the ordered structure in the course of deformation.[33] On the other hand, the 1.5/A sample, containing semi-coherent 9R structure, results in less improved YS but higher $\frac{d\sigma}{d\varepsilon}$ according to the generation of the geometrically necessary dislocations (GNDs) and back stresses from the Orowan loops.[33] Note that the area between the gauge length, next to the winding part of the sample was scanned for the spectra. This area is less susceptible to the deformation during the tensile testing.

One question still remains unanswered: the reason for the increased ductility. In the previous work, it was suggested that a strain-induced BCC-to-9R transformation occurs under tension similar to the TRIP-effect in TRIP-steels which adds an additional increment to the overall ductility.[1,13] However, the EXAFS modeling performed within this paper does not suggest the presence of mixed B2 and 9R precipitates in the sample 1.5/A but nearly pure 9R (93 atomic%) so that the latter hypothesis seems rather unlikely. A slightly smaller primary grain size of the austenite was detected in the previous work, which may have some effect on the ductility by means of grain refinement. Nonetheless, the exact reasons for the slightly increased ductility need to be studied thoroughly in future work.

6. Conclusions

EXAFS analysis by using the synchrotron XAS was successfully used for the first time to identify the unknown phases of copper precipitates in a copper-added martensitic 18CrNiMo7-6 steel where the states of peak strength could not be determined by means of tempering curves. The analysis helped explain the prior observed mechanical behavior by establishing microstructure-property correlation. Based on the performed analyses, the following can be concluded:

- The B2 ordered structure could be identified in the 18CrNiCuMo7-6 sample alloyed with 1 mass% copper and aged for 480°C for 50 minutes. This led to the highest improvement in yield strength but moderate increased strain hardening rate. After the overaging time of 240 minutes, the co-existence of the semi-coherent of 9R could be proven.
- Almost only the 9R structure of pure copper precipitates was detected in the 18CrNiMo7-6 samples alloyed with 1.5 mass% copper. A small amount of the B2 structure (6.9%) was found after aging at 500°C for 166 minutes. Only the 9R phase stayed stable after the long overaging time of 360 minutes. This structure resulted in the optimum strain hardening rate and ductility and is recommended for improving the damage tolerance of gearbox components.

Supporting Information

[CIF files of modeled copper precipitates structures for EXAFS]

This material is available on the Journal website at https://doi.org/10.2355/isijinternational.ISIJINT-2021-409.

Acknowledgements

The authors are grateful to some funding from King Mongkut's University of Technology North Bangkok (KMUTNB), grant number KMUTNB-61-KNOW-033 as well as Mr. Sayan Ruankon for his help with some artwork. The publication of this article was funded by the Open Access Fund of the Leibniz Association.

REFERENCES

1) A. Deschamps, M. Militzer and W. J. Poole: *ISIJ Int.*, **41** (2001), 196. https://doi.org/10.2355/isijinternational.41.196
2) E. Hornbogen and R. C. Glenn: *Trans. Metall. AIME*, **218** (1960), 1064.
3) S. R. Goodman, S. S. Brenner and J. R. Low: *Metall. Trans.*, **4** (1973), 2363. https://doi.org/10.1007/BF02669376
4) K. Osamura, H. Okuda, M. Takashima, K. Asano and M. Furusaka: *Mater. Trans., JIM*, **34** (1993), 305. https://doi.org/10.2320/matertrans1989.34.305
5) G. M. Worrall, J. T. Buswell, C. A. English, M. G. Hetherington and G. D. W. Smith: *J. Nucl. Mater.*, **148** (1987), 107. https://doi.org/10.1016/0022-3115(87)90525-3
6) P. J. Othen, M. L. Jenkins, G. D. W. Smith and W. J. Phythian: *Philos. Mag. Lett.*, **64** (1991), 383. https://doi.org/10.1080/09500839108215121
7) N. Maruyama, M. Sugiyama, T. Hara and H. Tamehiro: *Mater. Trans., JIM*, **40** (1999), 268. https://doi.org/10.2320/matertrans1989.40.268
8) M. K. Miller, K. F. Russell, P. Pareige, M. J. Starink and R. C. Thomson: *Mater. Sci. Eng. A*, **250** (1998), 49. https://doi.org/10.1016/S0921-5093(98)00535-8
9) P. J. Othen, M. L. Jenkins and G. D. W. Smith: *Philos. Mag. A*, **70** (1994), 1. https://doi.org/10.1080/01418619408242533
10) S. M. He, N. H. van Dijk, M. Paladugu, H. Schut, J. Kohlbrecher, F. D. Tichelaar and S. van der Zwaag: *Phys. Rev. B*, **82** (2010), 174111. https://doi.org/10.1103/PhysRevB.82.174111
11) K. Osamura, H. Okuda, S. Ochiai, M. Takashima, K. Asano, M. Furusaka, K. Kishida and F. Kurosawa: *ISIJ Int.*, **34** (1994), 359. https://doi.org/10.2355/isijinternational.34.359
12) M. D. Bambach, W. Bleck, H. S. Kramer, M. Klein, D. Eifler, T. Beck, H. Surm, H.-W. Zoch, F. Hoffmann and A. Radulescu: *Steel Res. Int.*, **87** (2016), 550. https://doi.org/10.1002/srin.201500129
13) M. D. Bambach: Ph.D. thesis, RWTH Aachen University, (2015).
14) M. Perez, F. Perrard, V. Massardier, X. Kleber, A. Deschamps, H. de Monestrol, P. Pareige and G. Covarel: *Philos. Mag.*, **85** (2005), 2197. https://doi.org/10.1080/14786430500079645
15) Y. R. Wen, Y. P. Li, A. Hirata, Y. Zhang, T. Fujita, T. Furuhara, C. T. Liu, A. Chiba and M. W. Chen: *Acta Mater.*, **61** (2013), 7726. https://doi.org/10.1016/j.actamat.2013.09.011
16) G. Han, Z. J. Xie, Z. Y. Li, B. Lei, C. J. Shang and R. D. K. Misra: *Mater. Des.*, **135** (2017), 92. https://doi.org/10.1016/j.matdes.2017.08.054
17) G. Han, Z. J. Xie, B. Lei, W. Q. Liu, H. H. Zhu, Y. Yan, R. D. K. Misra and C. J. Shang: *Mater. Sci. Eng. A*, **730** (2018), 119. https://doi.org/10.1016/j.msea.2018.05.080
18) W. Wang, B. Zhou, G. Xu, D. Chu and J. Peng: *Mater. Charact.*, **62** (2011), 438. https://doi.org/10.1016/j.matchar.2011.02.006
19) B. L. Chen, W. Wang, H. Xie, R. R. Ge, Z. Y. Zhang, Z. W. Li, X. Y. Zhou and B. X. Zhou: *J. Microsc.*, **262** (2016), 123. https://doi.org/10.1111/jmi.12352
20) H. A. Hardouin Duparc, R. C. Doole, M. L. Jenkins and A. Barbu: *Philos. Mag. Lett.*, **71** (1995), 325. https://doi.org/10.1080/09500839508241015
21) E.-S. M. A. Rassoul: *J. Mater. Sci.*, **32** (1997), 6471. https://doi.org/10.1023/A:1018694707380
22) J.-G. Jung, M. Jung, S.-M. Lee, E. Shin, H.-C. Shin and Y.-K. Lee: *J. Alloy. Compd.*, **553** (2013), 299. https://doi.org/10.1016/j.jallcom.2012.11.108
23) F. Maury, N. Lorenzelli, C. H. de Novion and P. Lagarde: *Scr. Metall. Mater.*, **25** (1991), 1839. https://doi.org/10.1016/0956-716X(91)90314-Q
24) S. Pizzini, K. J. Roberts, W. J. Phythian, C. A. English and G. N. Greaves: *Philos. Mag. Lett.*, **61** (1990), 223. https://doi.org/10.1080/09500839008202362
25) Y. Fujimura, H. Yoshizaki, S. Nakagawa, Y. Okamoto, N. Ishikawa, Y. Saitoh, F. Hori and A. Iwase: *Nucl. Instrum. Methods Phys. Res. B*, **354** (2015), 120. https://doi.org/10.1016/j.nimb.2014.11.043
26) P. Suwanpinij, H. H. Dickert, N. Thammajak and P. Srichareonchai: *Mater. Test.*, **58** (2016), 5. https://doi.org/10.3139/120.110802
27) J .P. Perdew and A. Zunger: *Phys. Rev. B*, **23** (1981), 5048. https://doi.org/10.1103/PhysRevB.23.5048
28) J. P. Perdew and Y. Wang: *Phys. Rev. B*, **45** (1992), 13244. https://doi.org/10.1103/PhysRevB.45.13244
29) G. Kresse and J. Furthmüller: *Comput. Mater. Sci.*, **6** (1996), 15. https://doi.org/10.1016/0927-0256(96)00008-0
30) H. J. Monkhorst and J. D. Pack: *Phys. Rev. B: Solid State*, **13** (1976), 5188. https://doi.org/10.1103/PhysRevB.13.5188
31) J. J. Rehr and R. C. Albers: *Rev. Mod. Phys.*, **72** (2000), 621. https://doi.org/10.1103/RevModPhys.72.621
32) L. Hedin and B. I. Lundqvist: *J. Phys. C: Solid State Phys.*, **4** (1971), 2064. https://doi.org/10.1088/0022-3719/4/14/022
33) M. F. Ashby: *Philos. Mag.*, **21** (1970), 399. https://doi.org/10.1080/14786437008238426